Int J Fract (2012) 177:97–108
DOI 10.1007/s10704-012-9757-4

ORIGINAL PAPER

Collapse and coalescence of spherical voids subject to intense shearing: studied in full 3D

Kim L. Nielsen · Jonas Dahl · Viggo Tvergaard

Received: 18 April 2012 / Accepted: 20 July 2012 / Published online: 10 August 2012

Abstract Micro-mechanical 2D cell model studies have revealed ductile failure during intense shearing to be governed by the interaction of neighbouring voids, which collapse to micro-cracks and continuously rotate and elongate until coalescence occurs. For a three-dimensional void structure, this implies significant straining of the matrix material located on the axis of rotation. In particular, the void surface material is severely deformed during shearing and void surface contact is established early in the deformation process. This 3D effect intensifies with decreasing stress triaxiality and complicates the numerical analysis, which is also reflected in published literature. Rather than moving towards very low triaxiality shearing, work has focused on extracting wide-ranging results for moderate stress triaxiality ($T \sim 1$), in order to achieve sufficient understanding of the influence of initial porosity, void shape, void orientation etc. The objective of this work is to expand the range of stress triaxiality usually faced in 3D cell model studies, such that intense shearing is covered, and to bring forward details on the porosity and void shape evolution. The overall material response is presented for a range of initial material configurations and loading conditions. In addition, a direct comparison to corresponding 2D cell model predictions for circular cylindrical voids under plane strain shearing is presented. A quantitatively good agreement of the two model configurations (2D vs. 3D) is obtained and similar trends are predicted. However, the additional layer of matrix material, connecting voids in the transverse direction, is concluded to significantly influence the void shape evolution and to give rise to higher overall ductility. This 3D effect is demonstrated for various periodic distributions of voids.

Keywords Voids · Low triaxiality · Shear deformation · Ductile failure · 3D effects

K. L. Nielsen (✉) · V. Tvergaard
Department of Mechanical Engineering, Solid Mechanics, Technical University of Denmark, 2800 Kgs. Lyngby, Denmark
e-mail: kin@mek.dtu.dk

J. Dahl
Department of Mechanical and Manufacturing Engineering, Aalborg University, 9220 Aalborg, Denmark

1 Introduction

Ductile failure by void nucleation, growth, and coalescence at high triaxiality stresses has been subject to extensive studies in the literature (Needleman 1972; Tvergaard 1982; Koplik and Needleman 1988; Gologanu et al. 1993, 1994; Benzerga 2002; Li and Steinmann 2006; Scheyvaerts 2008; Jodlowski 2011). The governing mechanisms are fairly well understood and their macroscopic effects are captured well by micro-mechanics based damage/coalescence models (Gurson 1977; Chu and Needleman 1980; Tvergaard 1981, 1982; Tvergaard and Needleman

1984; Thomason 1990; Gologanu et al. 1997; Pardoen and Hutchinson 2000; Lassance et al. 2007). In contrast, the mechanisms governing ductile *shear* failure, and the inability of the classical Gurson-type models to predict failure under intensive shearing, has only recently caught attention in the literature. It has been recognized that, at zero mean stress, the Gurson family models fail to predict the loss of load carrying capacity usually coming from an increased void volume fraction—thus, failure at zero mean stress cannot readily be predicted. To remedy this, Nahshon and Hutchinson (2008) suggested an extension to the Gurson model that accommodates failure under intense shearing by letting the damage parameter increase during plastic loading at zero mean stress. A softening effect from existing damage is thereby obtained when coalescence occurs (Tvergaard and Nielsen 2010). However, this artificial increase of damage in the Nahshon-Hutchinson-model is phenomenological, and the damage evolution is no longer tied to the void volume fraction. In fact, the closure of existing void (decreasing porosity) or delayed growth, predicted by the Gurson family models during shearing (Nielsen 2010), is clearly reflected in cell model studies (Tvergaard 2008, 2009; Barsoum and Faleskog 2011), and is easily detected as smeared dimples on fractographs. However, the combined effect of collapsed voids and the loss of load carrying capacity at zero mean stress is yet to be unified in one damage model.

Efforts have gone into the investigation of the governing factors in the void sheet mechanism and intense void shearing. E.g. the influence of inclusions, or debris hereof, on void shearing has been considered in the numerical investigations by Fleck et al. (1989), Tvergaard (1989), McVeigh et al. (2007). From the early studies it is known that contact araising between the particle and the void surface during shearing has a significant influence on the subsequent behaviour. This has also been recognized in the more recent study by McVeigh et al. (2007), seeking to encapsulate void nucleation, growth and coalescence in pure shear loading. For inclusions located in a periodic array, some signs of void interaction can be seen from their work, whereas coalescence was only obtained for clusters of particles. This is attributed the void growth phase which is crucial to the McVeigh-model, but is severely suppressed due to intense shearing.

To facilitate development of micro-mechanics based damage models towards accurately covering the full range of stress triaxiality loadings, a number of combined tension/shearing cell model studies of voided material, without inclusions, have been presented (Anderson et al. 1990; Barsoum and Faleskog 2007a,b; Tvergaard 2008, 2009; Leblond and Mottet 2008; Scheyvaerts 2008; Gao and Zhang 2010; Nielsen and Tvergaard 2011; Jodlowski 2011; Barsoum and Faleskog 2011; Tekoglu et al. 2012). In a recent series of studies on shearing of circular cylindrical voids at plane strain, Tvergaard and co-workers (Tvergaard 2008, 2009; Tvergaard and Nielsen 2010; Nielsen and Tvergaard 2011; Dahl et al. 2012), have shown that voids in a shear field undergo the following sequence of deformation steps; during shearing the voids are flattened out to micro-cracks, which continuously rotate and elongate until interaction with neighbouring micro-cracks gives coalescence. Consequently, a maximum load carrying capacity is attained due to interaction of micro-cracks. The work on void shear coalescence has been extended into full 3D by Barsoum and Faleskog (2007a), Barsoum and Faleskog (2007b), Scheyvaerts (2008), Barsoum and Faleskog (2011), Jodlowski (2011). In the work by Barsoum and Faleskog (2007a), Barsoum and Faleskog (2007b), Barsoum and Faleskog (2011), coalescence under combined tension and shear loading has been investigated by employing an experimental procedure together with 3D cell model calculations. The main focus of their work is the transition between rupture by internal necking and internal shearing, respectively, as-well as the influence of the Lode parameter on ductile failure. To date, it is widely accepted that besides the stress triaxiality additional quantities, such as the Lode parameter, is needed to describe the ductile failure process (Nahshon and Hutchinson, 2008; Gao and Zhang, 2010; Barsoum and Faleskog, 2011). In parallel to these, Scheyvaerts (2008) investigated, in full 3D, the shape evolution and rotation of voids subject to shear with particular interest in the first stage of the deformation in order to further extend the coalescence criterion by Thomason (1990). Recently, Jodlowski (2011) presented a comprehensive experimental investigation of void shearing in combination with full 3D modelling of void growth to coalescence.

Common to the published 3D cell model studies of pre-voided material is the fact that moderate stress triaxiality ($T \sim 1$) has been applied in terms of far field loading, while the low triaxiality regime has proven cumbersome for extensive parametric studies

due to limited void growth. The objective of the present work is to expand the range of stress triaxiality usually covered by 3D cell model studies, so that shearing under low stress triaxiality ($T \sim 0.1$) is covered, in order to enhance the understanding of the mechanisms governing ductile shear failure. Indications that the shear coalescence mechanism reported by Tvergaard (2008, 2009), may translate into full 3D can be found in Barsoum and Faleskog (2007a,b), Scheyvaerts (2008), Barsoum and Faleskog (2011), Jodlowski (2011), however the present work aims to conclusively demonstrate this for very low triaxiality. For doing so, a direct comparison of 2D (circular cylindrical voids) and 3D (spherical voids) cell model predictions is presented and details on the evolution of the void volume, shape, and orientation are brought out. In addition, this allows for a critical assessment, in terms of both quantitative and qualitative accuracy, of previously published 2D results on shear coalescence. Moreover, the 3D effects primarily responsible for the quantitative deviations are pointed out. For clarity of results, the study is limited to shearing of existing spherical voids in an isotropic matrix material. Thus, effects of the initial voids shape/orientation and matrix material an-isotropy are yet to be studied in details.

The paper is structured as follows. The employed micro-mechanical model is outlined in Sect. 2, while the numerical modelling approach and material model are presented in Sect. 3. Focus is on the developed 3D cell model, whereas details on the corresponding 2D model are omitted, with suitable references. Results are presented in Sect. 4, where the collapse of spherical voids is illustrated and 3D cell model predictions are compared to corresponding 2D cell model predictions for circular cylindrical voids. The concluding remarks are given in Sect. 5.

2 Micro-mechanical model

Continuing along the work on shear coalescence initiated by Tvergaard (2008, 2009), the current 3D cell model study and the numerical studies by Barsoum and Faleskog (2007a,b), Scheyvaerts (2008), Jodlowski (2011) rest on common ground. A periodic array of voids located in the x_1x_3-plane of a bulk material, subject to intense shearing in the x_1x_2-plane (see Fig. 1), is considered in order to analyze the void coalescence mechanism in details. Throughout, the onset of void coalescence is associated with the loss of material load carrying capacity. Thus, coalescence is defined as where the peak load is attained. The discretely modelled voids are initially spherical with radius R_0, and with void spacing $2A_0$ in the x_1-direction, $2B_0$ in the x_2-direction and $2C_0$ in the x_3-direction ($B_0/A_0 = 4$ for all results presented). According to the 2D cross-section highligted in Fig. 1a, periodic boundary conditions are applied along the left ($x_1 = -A_0$) and the right ($x_1 = A_0$) plane of the cell so that $u_i(-A_0, x_2, x_3) = u_i(A_0, x_2, x_3)$, with $i = 1, 2, 3$. The periodic arrangement of voids in the x_3-direction are imposed by symmetry conditions so that $u_3(x_1, x_2, 0) = u_3(x_1, x_2, -C_0) = 0$. All periodic boundary conditions are enforced through the displacement field, whereby the tractions naturally fall out of the finite element formulation.

Here, the top/bottom of the domain remains plane and in their original orientation, thus interaction between rows of micro-voids is neglected. This is an approximation and the effect of B_0/A_0 on the overall shear angle; $\tan(\psi) = U_I/(B_0 + U_{II})$, is thereby neglected. Another approach would be to employ a periodically repeated unit cell in the x_2-direction, and thereby account for interaction in that direction. In a recent study, Tvergaard (2012) compares these two model settings and shows that the effect on the peak load is negligible for $B_0/A_0 > 2$, whereas only the post-localization behavior displays noticeable differences.

An incremental load is applied along the top ($x_2 = B_0$) and the bottom ($x_2 = -B_0$) planes of the volume, so that

$$\dot{u}_1 = \dot{U}_I, \quad \dot{u}_2 = \dot{U}_{II} \quad \text{for} \quad x_2 = B_0 \tag{1}$$

$$\dot{u}_1 = -\dot{U}_I, \quad \dot{u}_2 = -\dot{U}_{II} \quad \text{for} \quad x_2 = -B_0. \tag{2}$$

Here $\dot{U}_I$ is the prescribed deformation rate in the x_1-direction, while $\dot{U}_{II}$ is continuously corrected so that an average stress ratio $\kappa = \sum_{22} / \sum_{21}$ for the far field loading is maintained throughout the calculation. The average stress at the top and bottom surface are calculated as

$$\sum_{22} = \frac{1}{2A_0C_0} \int_{-C_0}^{0} \int_{-A_0}^{A_0} T_2 \mathrm{d}x_1 \mathrm{d}x_3, \tag{3}$$

$$\sum_{21} = \frac{1}{2A_0C_0} \int_{-C_0}^{0} \int_{-A_0}^{A_0} T_1 \mathrm{d}x_1 \mathrm{d}x_3, \tag{4}$$

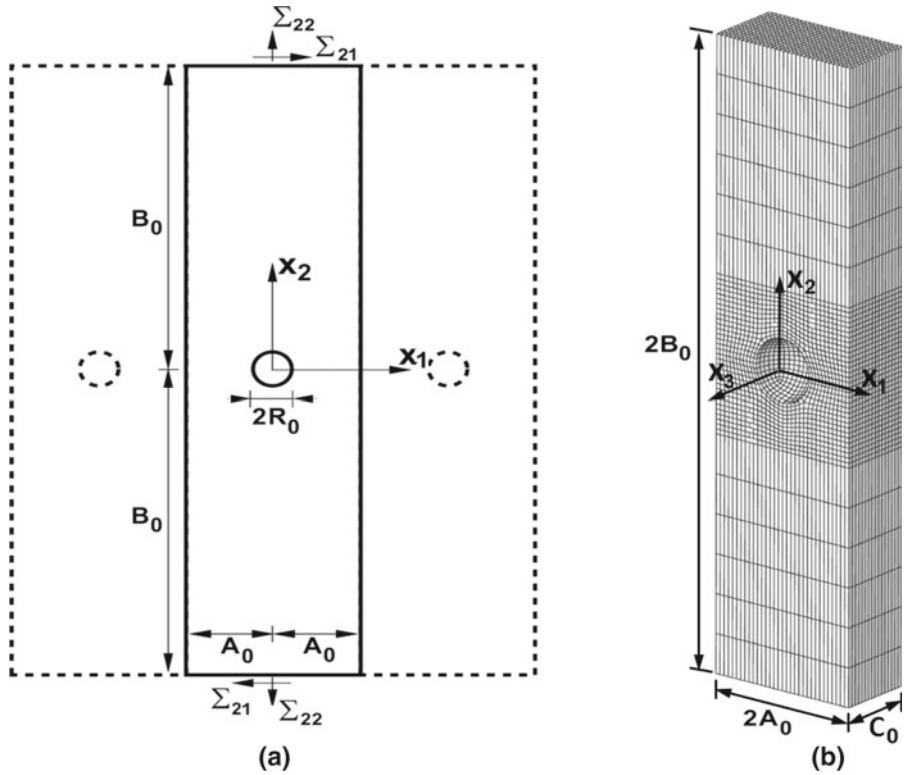

Fig. 1 Periodic array of spherical voids with radius R_0 and void spacing $2A_0$, $2B_0$ and $2C_0$ in the x_1-, x_2-, and x_3-direction, respectively, showing **a** the array of voids and applied shear stress ratio ($\kappa = \sum_{22} / \sum_{21}$) in the x_1x_2-plane, and **b** a representative mesh used in modelling shear coalescence ($B_0/A_0 = 4$ for all results presented)

for $x_2 = \pm B_0$, with T_i being the nominal surface tractions. In the present study, a far field stress ratio as low as $\kappa = 0.25$ (thus $T \approx 0.089$) has been made possible in the 3D model by taking into account void surface contact. However, values lower than $\kappa = 0.25$ have given rise to numerical difficulties and termination of the calculations, in particular for small void sizes.

3 Model: constitutive relation and numerical procedure

The boundary value problem posed in Sect. 2 is solved using the finite element code ABAQUS/explicit (2010). The following Sects. 3.1–3.2 present the applied constitutive material model and the numerical model set-up. Where clarity of the paper is not sacrificed, previously published details of the constitutive model and the finite strain elastic-plastic formulation will be omitted, with suitable references.

3.1 Constitutive model

The finite strain formulation for the applied J_2-flow theory material with the Mises yield surface, employs the incremental stress-strain relationship; $\dot{\sigma}_{ij} = L_{ijkl}\dot{\varepsilon}_{kl}$, where; σ_{ij} is the Cauchy stress, $\varepsilon_{ij} = (u_{i,j} + u_{j,i})/2$ is the total strain, and L_{ijkl} are the instantaneous moduli (ABAQUS 2010). Here, the total strain increment is taken to be the sum of an elastic and a plastic parts; $\dot{\varepsilon}_{ij} = \dot{\varepsilon}^E_{ij} + \dot{\varepsilon}^p_{ij}$. According to the updated Lagrangian formulation all integrations are carried out in the deformed configuration. The true stress-logarithmic strain curve in uni-axial tension of the matrix material is taken as

$$\varepsilon = \begin{cases} \sigma/E, & \text{for } \sigma < \sigma_Y \\ \sigma_Y/E\,(\sigma/\sigma_Y)^{1/N}, & \text{for } \sigma \geq \sigma_Y \end{cases} \tag{5}$$

where E is Young's modulus, σ_Y is the initial yield stress and N is the power hardening exponent, while σ is identified as the von Mises stress, $\sigma_e = (3/2 s_{ij}s_{ij})^{1/2}$, for the multi-axial stress state, and s_{ij} is the Cauchy

Table 1 Mechanical properties

Parameter	Significance	Value
E	Young's modulus	200 GPa
ν	Poisson's ratio	0.3
ρ	Mass density	7,800 kg/m^3
σ_Y	Initial yield stress	400 MPa
N	Strain hardening exponent	0.1–0.2

stress deviator. The material is taken to be isotropic hardening. The simple power hardening law in Eq. (5) is chosen to limit the number of model parameters, but more realistic hardening laws (e.g the Voce law typically used for aluminum, Simar et al. 2010) could equally well be used for the analyses. All material parameter values are given in Table 1.

3.2 Numerical procedure

A numerical solution is obtained by the commercial FE-code ABAQUS/explicit (2010), using an explicit dynamic model formulation in an updated Lagrangian framework. To avoid effects of material inertia, due to a sudden prescribed displacement, the deformation rate $\dot{U}_I$ is ramped up, while the deformation rate $\dot{U}_{II}$ is continuously adjusted so that the average stress ratio, κ, is maintained. This is obtained through a standard proportional regulation algorithm, which offers sufficient accuracy for the purpose of the current analysis.

The domain governed by the field equations is discretized by 8 node isoparametric 3D solid elements, using reduced Gauss quadrature for the spatial integration. Here, a standard forward Euler procedure is employed for the time integration, with a lumped mass matrix to decouple the system of equations and lower the calculation time in each increment. A convergence study shows that this dynamic approach gives a very good approximation to the static solution under slow loading.

3.2.1 Adaptive meshing

In ABAQUS, the dynamic approach has the advantage over a static analysis that the Arbitrary Lagrangian-Eulerian (ALE) method, that adjusts the mesh according to the deformation of the underlying material, is more robust. This is important when accounting for the severe material flow around the crack tip of a completely flattened void. The ALE mesh adaptive method is used to avoid excessive distortion of elements which leads to inaccuracy of the results and often to termination of the analysis. In particular, this is important to accurately account for the material flow that occurs in the vicinity of the crack tips. In all of the analyses presented, three ALE mesh sweeps per time increment are performed to limit distortion of the mesh. All other ALE options are the ABAQUS (2010) default. However, to facilitate enforcement of the periodic boundary conditions the ALE mesh smoothing is made in-active at the cell boundaries (see e.g. Dahl et al. 2012, for further details).

3.2.2 Contact procedure

To account for contact between the void surfaces, the ABAQUS general contact formulation is employed. Using a standard penalty based contact formulation (see e.g. Belytschko et al. 2000), penetration of one surface into another can be avoided by using a master-slave setup. The ABAQUS general contact formulation first treats one of the surfaces as the master and the other surface as the slave. Adequate penalty forces are thereby calculated to avoid penetration, whereafter the master/slave roles are interchanged and a new set of penalty forces are calculated. The actual penalty forces used in the next time increment are a weighted average of the two. Thus, the contact algorithm does not avoid penetration of the surfaces, but for the analyses conducted the observed penetrations are negligible. Throughout, only frictionless contact is considered (see Dahl et al. 2012, for further details on the effects of friction).

4 Results

4.1 Material response and load carrying capacity of a 3D void structure

The overall response of a bulk material containing a periodic array of spherical voids is presented in Figs. 2a and 3a for various void sizes, R_0/A_0, and void spacings, C_0/A_0, respectively, and the corresponding critical shear angles, ψ_C, for which the peak load is attained, are presented in Figs. 2b and 3b. Clearly, the response of the current full 3D cell model resembles that of

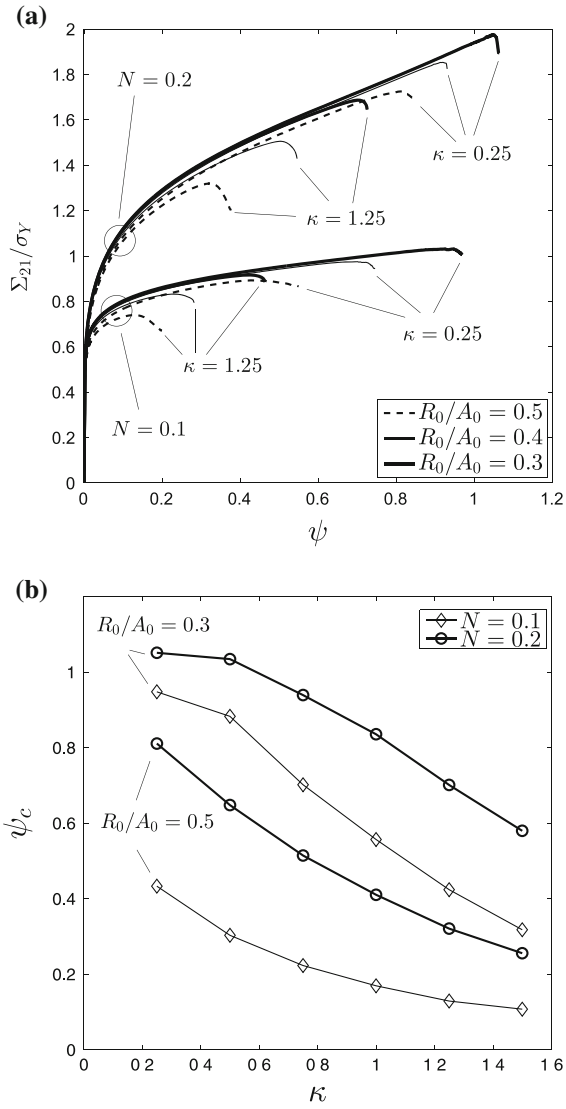

Fig. 2 Overall material response of bulk material containing a periodic array of spherical voids, showing **a** average shear stress versus average shear angle for various void sizes, $R_0/A_0 = [0.3, 0.4, 0.5]$, subject to shearing, $\kappa = [1.25, 0.25]$, and **b** corresponding critical average shear angle, ψ_C, at the onset of coalescence (peak load) versus applied stress ratio, κ, for $R_0/A_0 = [0.3, 0.5]$ ($N = [0.1, 0.2]$, $C_0/A_0 = 1$, $\sigma_y/E = 0.002$ and $\nu = 0.3$)

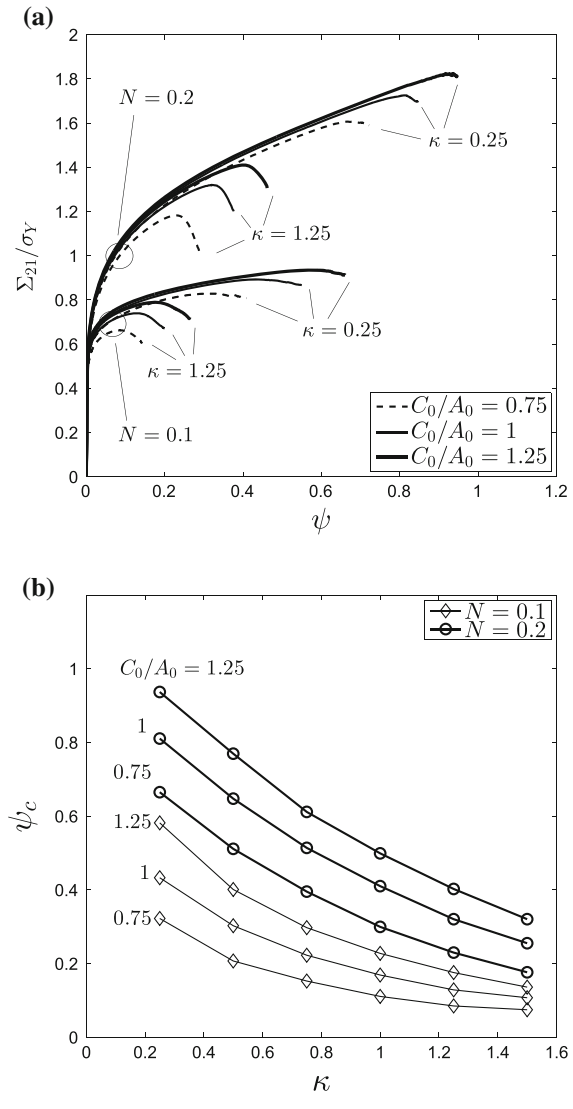

Fig. 3 Overall material response of bulk material containing a periodic array of spherical voids, showing **a** average shear stress versus average shear angle for various void spacings in the x_3-direction, $C_0/A_0 = [0.75, 1, 1.25]$, subject to shearing, $\kappa = [1.25, 0.25]$, and **b** corresponding critical average shear angle, ψ_C, at the onset of coalescence (peak load) versus applied stress ratio, κ ($R_0/A_0 = 0.5$, $N = [0.1, 0.2]$, $\sigma_y/E = 0.002$ and $\nu = 0.3$)

the 2D model proposed by Tvergaard (2008, 2009), and the aim to further quantify this will be pursued in Sect. 4.3. Similar to published 2D model predictions, the overall material ductility is found to increase with decreasing void size, R_0/A_0 (decreasing initial porosity), and to increase with strain hardening, N. Thus, the current 3D cell model predictions follow the recognized behaviour of voided material subject to combined tension and shearing. Moreover, the overall material ductility is predicted to increase severely for low triaxiality shearing. In particular, this is evident from Figs. 2b and 3b, where the critical shear angle, ψ_C, shows a monotonic increase with decreasing far field stress ratio, $\kappa = \sum_{22} / \sum_{21}$. Only a slight deviation

from this common trend is observed from Fig. 2b for $R_0/A_0 = 0.3$, when $\kappa < 0.5$. In a closer examination, it was found that only this combination of material configuration and loading condition shows a complete closure of the void mid-section during collapse (see also Sect. 4.2). It should be noticed that, a few recent experimental studies have shown that the strain-to-failure is not a monotonic function of stress triaxiality (Bao and Wierzbicki, 2004; Barsoum and Faleskog, 2007a), as a peak strain is attained at moderate levels. This effect has not been captured in the current analysis, and to the authors knowledge, a conclusive study on this phenomenon is yet to be published.

The effect of the additional matrix material connecting voids in the x_3-direction is brought out in Fig. 3. It is observed that this dense layer of material has a significant influence on the overall ductility (see Fig. 3b), and that the response for various C_0/A_0-spacings closely follows one master curve until the onset of coalescence (see Fig. 3a). Thus, changes in void size, R_0/A_0, and void spacing, C_0/A_0, share the same effect on the material response and the onset of coalescence (compare Figs. 2a and 3a). This is attributed to interference of stress-strain fields surrounding the individual voids—or the lack hereof. In the limit $C_0/A_0 \to \infty$ (or $R_0/A_0 \to 0$), voids will become isolated and there will be no failure. Thus, for increasing but still limited void spacing, C_0/A_0 (or decreasing R_0/A_0), a larger average shear angle, ψ, should be applied in order to maintain the stress/strain level in the matrix material located on the cell boundaries—thus, the overall ductility increases.

4.2 Collapse and coalescence of spherical voids

In contrast to tension dominated conditions, where void growth initially softens the material, it is the void shape change and the void volume collapse that contributes to a softening effect during low triaxiality shearing. Figure 4 demonstrates the sequence of deformation steps typically observed for spherical voids in a shear field prior to void coalescence. During very low triaxiality shearing, the voids initially take on a prolate shape (see Fig. 4b), and continuously rotate and elongate, while collapsing into micro-cracks (see Fig. 4c). During this deformation, large plastic straining occurs along the rim of the voids. In particular, the void surface material, located on the axis of rotation, experiences severe straining and void surface contact is established early in the shearing process (near $x_3 = -R_0$ for the undeformed void, see Fig. 4c). Upon further shearing, the voids are flattened completely and the area in contact evolves such that the mid-section of the voids close-up, leaving only the crack-tips open (see Fig. 4d). This void collapse is substantially delayed in the 3D study of Fig. 4, due to the dense layer connecting voids in the x_3-direction, and is the primary reason for deviations between the 2D and 3D model results. In the final stage of shearing, void coalescence sets in as interaction between neighbouring micro-cracks takes place and thinning of the ligaments occurs. As a consequence, a peak load is attained. This renders the overall sequence of deformation steps governing the shear coalescence mechanism for 3D spherical voids very similar to that reported for 2D circular cylindrical voids.

The early flattening of the initial spherical/circular cylindrical voids allows for the identification of a major, R_1, and a minor, R_2, void half axis located in the symmetry plane (x_1, x_2), as-well as a third axis, R_3, perpendicular to the x_1x_2-plane (in 3D). Here, R_1 is determined from the largest distance between nodes being part of the void surface (based on nodal coordinates), while R_2 is perpendicular to R_1. By doing so, the evolution of i) the void volume, V/V_0, ii) the void orientation specified by the angle, θ, between the major axis and the positive x_1-axis, and iii) the void shape in terms of the elongation/shortening of the void axes, can be visualized (see Fig. 5). For materials containing spherical voids, the following general observations are made for the shape evolution during shearing; as shearing takes place voids initially become prolate, and start to rotate from an approximately 45° angle towards the x_1-axis (this rotation is rather continuous and the sudden "jumps" seen from Fig. 5 is an artifact of the procedure used to extract the major axis, R_1). During the flattening and rotation of voids, the major and third axes elongate for all loading conditions considered, whereas the minor axis is shortened. As will be presented, this agrees well with 2D model predictions (see Sect. 4.3). In addition, it is observed that the rate of deformation of the void axes R_1 and R_3 increase with κ, while the opposite applies to the minor axis, R_2. Thus, the void rapidly becomes very long for high κ-values, but maintains low aspect ratios (R_1/R_2 and R_3/R_2), due to void growth, when compared to the case of very low triaxiality shearing. Moreover, an intriguing observa-

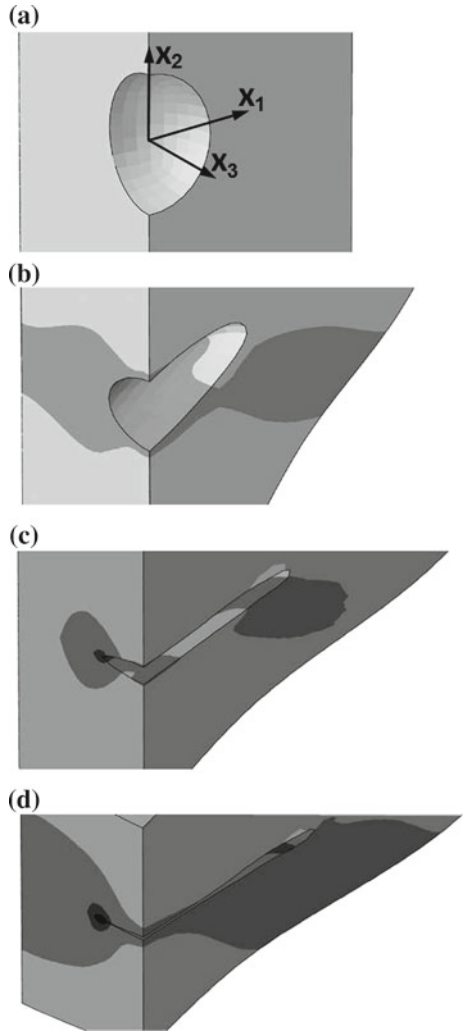

Fig. 4 Curves of constant effective plastic strain, ε_e^p, at **a** $\psi = 0$, **b** $\psi = 0.61$, **c** $\psi = 0.91$, and **d** $\psi = 1$ (just before coalescence) for $\kappa = 0.25$ ($R_0/A_0 = 0.3$, $C_0/A_0 = 1$, $N = 0.2$, $\sigma_y/E = 0.002$ and $\nu = 0.3$)

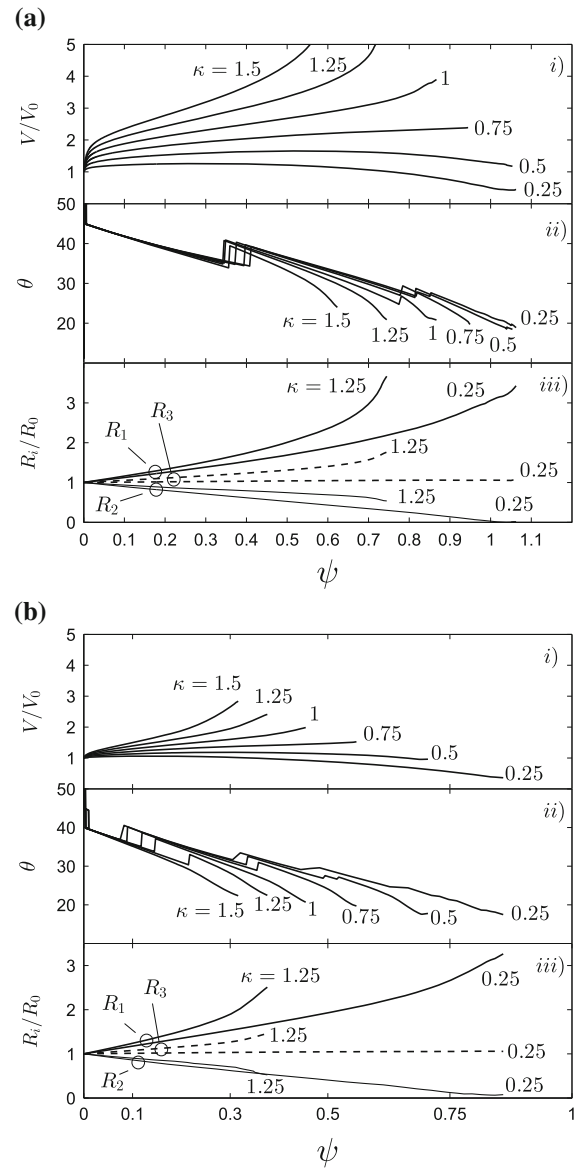

Fig. 5 Evolution of i) the void volume, V/V_0, ii) the void orientation specified by the angle, θ, between the major axis and the positive x_1-axis, and iii) the void shape in terms of the tree void axes, (R_1, R_2, R_3), as function of average shear angle. Here, showning the influence of loading conditions and initial void size **a** $R_0/A_0 = 0.3$, and **b** $R_0/A_0 = 0.5$ ($C_0/A_0 = 1$, $\kappa = [0.25, 0.5, 0.75, 1, 1.25, 1.5]$, $N = 0.2$, $\sigma_y/E = 0.002$ and $\nu = 0.3$)

tion is that the rate of rotation (or $\partial\theta/\partial\psi$) increases with κ, even though the void flattening becomes less intense (see Fig. 5ii, iii).

For the case of very low triaxiality shearing, $\kappa = 0.25$, Fig. 5 clearly shows that the initial void volume collapses (see Fig. 5i), while the void starts to rotate towards the x_1-axis. During the collapse, the major axis elongates, while the minor axis is shortened and the third axis remains nearly unchanged. Thus, the collapsed void forms an elongated penny-shaped microcrack (see Fig. 5iii). In contrast to this, a comparably large amount of void growth is predicted for the case of combined tension and shearing with $\kappa = 1.25$ (see Fig. 5i), which is also reflected in the shape evolution as both the major and transverse axes elongate, while the minor axis is slightly shortened (see Fig. 5iii).

4.3 Assessment of published 2D model predictions by direct comparison

The preceding discussion clearly reveals the coalescence mechanism for spherical voids (3D model) to fall into the sequence of deformation steps first reported by Tvergaard (2008, 2009) for circular cylindrical voids under plane strain conditions (2D model). In the following, a further assessment of the predictive capabilities of the 2D model, in terms of material response and micro-mechanics based parameters (void volume, shape and orientation), is presented with a direct comparison to the current 3D model set-up. For an accurate comparison, identical numerical procedure and contact algorithm are employed in both models. Thus, the 2D model follows the set-up presented in Dahl et al. (2012).

Figure 6 compares the predicted material response of a bulk material containing a periodic array of spherical voids (3D model), to a similar material with circular cylindrical voids (2D model). Two different model set-ups are here considered, for which; 1) the void size, R_0/A_0, is kept constant to compare the influence of model parameters, and 2) the void volume fraction is kept constant, $f_0^{2D} = f_0^{3D}$, to compare identical material configurations. The porosity associated with a row of voids is, however, not uniquely defined, thus it is approximated by the porosity associated with a band of width $2A_0$ in the x_2-direction (equal to the void spacing in the x_1-direction). Hence, the porosity can be expressed as $f_0^{2D} = \pi R_0^2/(4A_0^2)$ and $f_0^{3D} = \pi R_0^3/(6A_0^2 C_0)$ in the 2D and 3D models, respectively.

In the case of constant void size, R_0/A_0, it is found that the 2D model severely underestimates both the overall ductility and the load carrying capacity predicted by the 3D model. The inconsistency in the predicted material ductility is brought out in Fig. 7 for a close examination. Here, the critical average shear angle, ψ_C, at the onset of coalescence (peak load) is shown as function of the applied far field stress ratio, κ, for the 2D and 3D model, respectively. It is seen from Fig. 7 that the underestimation by the 2D model is rather significant and inconsistent with 3D model predictions. This is attributed an early collapse of 2D circular cylindrical voids, occurring as plastic flow localizes in the ligaments between neighbouring voids, whereas the corresponding localization is delayed by the additional material in the x_3-direction for spherical voids (see Sect. 4.3 and Fig. 4). Consequently, a substantially lower peak load should be expected for the 2D circular cylindrical voids.

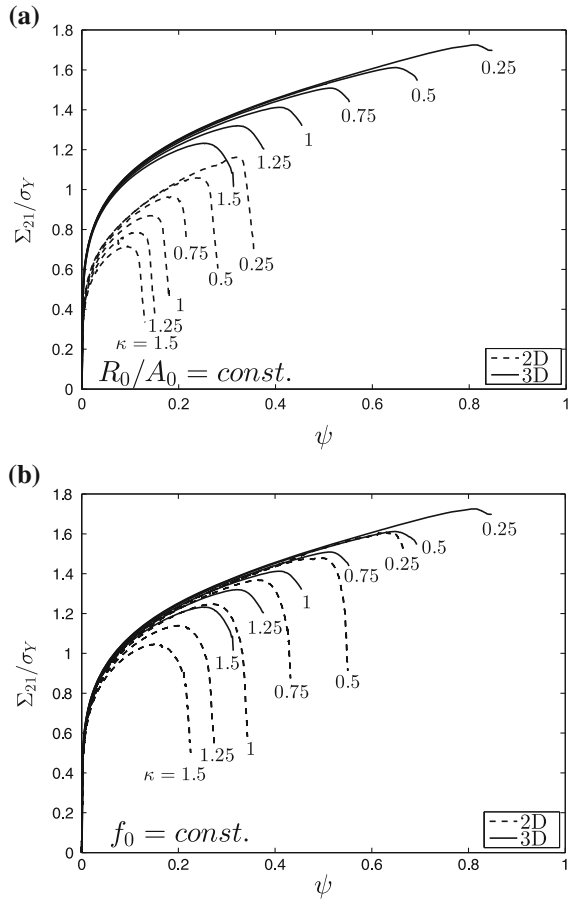

Fig. 6 Average shear stress versus average shear angle for spherical voids (*solid line*, 3D) and circular cylindrical voids at plane strain (*dashed line*, 2D). Here, shown for **a** constant void size $R_0/A_0 = 0.5$, and **b** approximate constant initial void volume fraction, f_0 ($\kappa = [0.25, 0.5, 0.75, 1, 1.25, 1.5]$, $N = 0.2$, $\sigma_y/E = 0.002$ and $\nu = 0.3$. Moreover, $C_0/A_0 = 1$ in 3D)

By introducing approximately identical porosities in the two models, $f_0^{2D} = f_0^{3D}$, a much better agreement is obtained (see Fig. 6b). In fact, the overall material response nearly follows one master curve, while the underestimation of the ductility is much reduced. This is also obvious from Fig. 7, where the 2D and 3D model predict curves of nearly identical appearance and with a close to constant offset.

Further details on the micro-mechanics governing the good agreement for the case of constant f_0 is revealed in Fig. 8. Here, the evolution of i) the void volume, V/V_0, ii) the void orientation, θ, and iii) the void

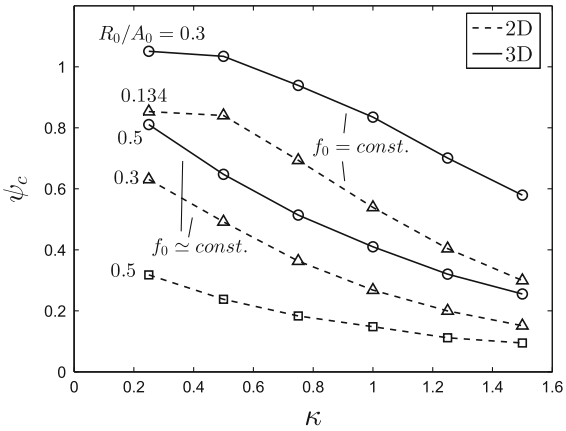

Fig. 7 Critical average shear angle at the onset of coalescence ($\psi = \psi_C$) versus applied stress ratio, κ, comparing predictions for spherical voids (*solid lines*, 3D) and circular cylindrical voids at plane strain (*dashed lines*, 2D). Curves of constant void spacing ($R_0/A_0 = [0.3, 0.5]$) for the 2D and the 3D model are presented, together with curves of constant approximated porosity, f_0 ($R_0/A_0|_{3D} = 0.5 \rightarrow R_0/A_0|_{2D} = 0.29$ and $R_0/A_0|_{3D} = 0.3 \rightarrow R_0/A_0|_{2D} = 0.134$), ($N = 0.2, \sigma_y/E = 0.002, \nu = 0.3$. Moreover, $C_0/A_0 = 1$ in 3D)

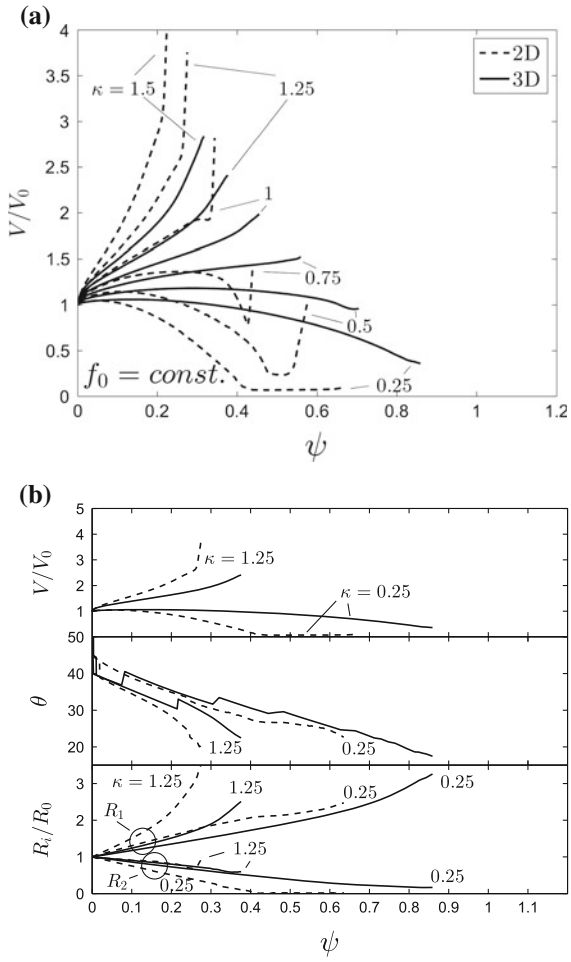

Fig. 8 **a** Void volume versus average shear angle for various far field stress ratios, κ, and **b** evolution of the i) void volume, V/V_0, ii) void orientation specified by the angle, θ, between the major axis and the positive x_1-axis, and iii) void shape in terms R_1, R_2 and R_3 as function of average shear angle for $\kappa = [0.25, 1.25]$. Here, comparing predictions for spherical voids (*solid line*, 3D) and circular cylindrical voids at plane strain (*dashed line*, 2D), with $f_0^{2D} = f_0^{3D}$ ($R_0/A_0 = 0.5$ in 3D and $R_0/A_0 = 0.29$ in 2D), ($N = 0.2$, $\sigma_y/E = 0.002$ and $\nu = 0.3$. Moreover, $C_0/A_0 = 1$ in 3D)

shape, R_i, is presented for both models. It is seen from Fig. 8a, that the 2D model predicts the void volume to collapse at a higher rate under very low triaxiality shearing ($\kappa = 0.25$) than the 3D model, whereas the opposite applies when the loading is composed of shearing and sufficient tension ($\kappa > 0.75$). Thus, the void volume evolution is clearly constrained in 3D. Again, this can be ascribed to the dense material layer connecting voids in the x_3-direction, which forces the void to remain slightly open at much larger overall shear deformations (see Fig. 4). This constraint is also reflected in Fig. 8b, as changes in the void axes occur somewhat more slowly in 3D. However, a rather good agreement between the 2D and 3D model is found for both the void orientation and the shape evolution—especially for the case of very low triaxiality shearing $\kappa = 0.25$.

5 Concluding remarks

Coalescence of spherical voids subject to low stress triaxiality shearing is studied with focus on widening the interval of triaxialities usually faced in 3D cell model studies, and adding to the understanding of the sequence of events leading to loss of load carrying capacity for ductile materials. Continuing along the work by Tvergaard (2008, 2009), Dahl et al. (2012), a 3D cell model has been developed and exploited in this investigation. The key findings of the study are:

– The material response for a bulk material containing a periodic array of spherical voids is illustrated for various initial material configurations (R_0/A_0, C_0/A_0, N), and loading conditions, κ. A significant influence of the additional dense material layer connecting voids in the x_3-direction is revealed and

gives a constraint on the void volume and shape evolution, as-well as toughens the material response in 3D. Thus, changes in the void size, R_0/A_0, and the void spacing C_0/A_0, are shown to share the same effect on the material response and the onset of coalescence (see Figs. 2, 3).

– The governing mechanisms for void coalescence under low triaxiality shearing, first brought out by Tvergaard (2008, 2009) for circular cylindrical voids, are demonstrated for spherical voids in full 3D. The primary sequence of deformation steps, in terms of void collapse, rotation and elongation, is shown to translate directly to a three-dimensional voided structure. Compared to the 2D model, the main difference lies in the shearing of the additional dense material layer in the transverse direction. During shearing of initially spherical voids, significant straining of the material located on the axis of rotation takes place and void surface contact is established rather early near $x_3 = -R_0$ (according to Fig. 1). This constricts the void collapse such that a complete closure is only obtained under very low triaxiality shearing. Moreover, the evolution of the void shape and orientation is brought out in the presented study (see Fig. 5).
– A comparison between 2D and 3D cell model predictions shows a good agreement when the void volume fraction is kept constant ($f_0^{2D} = f_0^{3D}$). In fact, the material response nearly follows one master curve, while the overall ductility is found to be underestimated in a consistent manner for a wide range of loading conditions and material configurations (see Figs. 6, 7). Moreover, a qualitatively good agreement between the 2D and 3D model is observed for the evolution of micro-mechanics based parameters such as; void volume, shape and orientation. Based on these findings, previously published results from 2D cell models can be viewed (with caution) as trend lines for corresponding 3D cell model predictions when keeping the void volume fraction approximately constant ($f_0^{2D} = f_0^{3D}$, see Sect. 4.3).

Acknowledgments KLN is financially support by the Danish Council for Independent Research under the research career programme Sapere Aude in the project "Higher Order Theories in Solid Mechanics".

References

ABAQUS (2010) ABAQUS Theory Manual, version 6.10, SIMULIA Corp

Anderson P, Fleck N, Johnson K (1990) Localization of plastic deformation in shear due to micro-cracks. J Mech Phys Solids 38:681–699

Bao Y, Wierzbicki T (2004) On fracture locus in the equivalent strain and stress triaxiality space. Int J Mech Sci 46:81–98

Barsoum I, Faleskog J (2007a) Rupture mechanisms in combined tension and shear—experiments. Int J Solids Struct 44:1768–1786

Barsoum I, Faleskog J (2007b) Rupture mechanisms in combined tension and shear—micromechanics. Int J Solids Struct 44:5481–5498

Barsoum I, Faleskog J (2011) Micromechanical analysis on the influence of the lode parameter on void growth and coalescence. Int J Solids Struct 48:925–938

Belytschko T, Liu W, Moran B (2000) Nonlinear finite elements for continua and structures. Wiley, New York

Benzerga A (2002) Micromechanics of coalescence in ductile fracture. J Mech Phys Solids 50:1331–1362

Chu A, Needleman A (1980) Void nucleation effects in biaxially stretched sheets. J Eng Mater Technol 102:249–256

Dahl J, Nielsen K, Tvergaard V (2012) Effect of contact conditions on void coalescence at low stress triaxiality Shearing. J Appl Mech. doi:10.1115/1.4005565

Fleck N, Hutchinson J, Tvergaard V (1989) Softening by void nucleation and growth in tension and shear. J Mech Phys Solids 37:515–540

Gao X, Zhang G (2010) A study on the effect of the stress state on ductile fracture. Int J Damage Mech 19:75–94

Gologanu M, Leblond J, Devaux J (1993) Approximate models for ductile metals containing nonspherical voids—case of axisymmetrical prolate ellipsoidal cavities. J Mech Phys Solids 41:1723–1754

Gologanu M, Leblond J, Devaux J (1994) Approximate models for ductile metals containing nonspherical voids—case of axisymmetrical oblate ellipsoidal cavities. J Eng Mater Technol 116:290–297

Gologanu M, Leblond J, Perrin G, Devaux J (1997) Recent extensions of Gurson's model for porous ductile metals. In: Continuum micromechanics, Springer, Berlin, pp 61–106

Gurson A (1977) Continuum theory of ductile rupture by void nucleation and growth—part I: yield criteria and flow rules for porous ductile media. ASME J Eng Mater Technol 99:2–15

Jodlowski T (2011) Mechanics of growth and coalescence of pre-existing voids in a ductile matrix. PhD thesis, École polytechnique fédérale de lausanne, Université de Lausanne

Koplik J, Needleman A (1988) Void growth and coalescence in porous plastic solids. Int J Solids Struct 24:835–853

Lassance D, Fabrègue D, Delannay F, Pardoen T (2007) Micromechanics of room and high temperature fracture in 6xxx Al alloys. Prog Mater Sci 52:62–129

Leblond JB, Mottet G (2008) A theoretical approach of strain localization within thin planar bands in porous ductile materials. C R Mecanique 336:176–189

Li Z, Steinmann P (2006) RVE-based studies on the coupled effects of void size and void shape on yield behavior and void growth at micron scales. Int J Plast 22:1195–1216

McVeigh C, Vernerey F, Wing K, Moran B, Olson G (2007) An interactive micro-void shear localization mechanism in high strength steels. J Mech Phys Solids 55:225–244

Nahshon K, Hutchinson J (2008) Modification of the Gurson model for shear. Euro J Mech A/Solids 27:1–17

Needleman A (1972) Void growth in an elastic-plastic medium. J Appl Mech 39:964–970

Nielsen K (2010) Predicting failure response of spot welded joints using recent extensions to the Gurson model. Comp Mater Sci 48:71–82

Nielsen K, Tvergaard V (2011) Failure by void coalescence in metallic materials containing primary and secondary voids subject to intense shearing. Int J Solids Struct 48:1255–1267

Pardoen T, Hutchinson J (2000) An extended model for void growth and coalescence. J Mech Phys Solids 48:2467–2512

Scheyvaerts F (2008) Multiscale modeling of ductile fracture in heterogeneous metallic alloys. PhD thesis, École polytechnique de Louvain, Université catholique de Louvain

Simar A, Nielsen K, de Meester B, Tvergaard V, Pardoen T (2010) Micro-mechanical modeling of ductile failure in 6005A aluminium using a physics based strain hardening law including stage IV. Eng Frac Mech 77:2491–2503

Tekoglu C, Leblond JB, Pardoen T (2012) A criterion for the onset of void coalescence under combined tension and shear (submitted)

Thomason P (1990) Ductile fracture of metals. Pergamon press, Oxford

Tvergaard V (1981) Influence of voids on shear band instabilities under plane strain conditions. Int J Fract 17:389–407

Tvergaard V (1982) On localization in ductile materials containing spherical voids. Int J Frac 18:237–252

Tvergaard V (1989) Numerical study of localization in a void-sheet. Int J Solids Struct 25:1143–1156

Tvergaard V (2008) Shear deformation of voids with contact modelled by internal pressure. Int J Mech Sci 50:1459–1465

Tvergaard V (2009) Behaviour of voids in a shear field. Int J Fract 158:41–49

Tvergaard V (2012) Effect of stress-state and spacing on voids in a shear-field (to appear)

Tvergaard V, Needleman A (1984) Analysis of the cup-cone fracture in a round tensile bar. Acta Metall 32:157–169

Tvergaard V, Nielsen K (2010) Relations between a micro-mechanical model and a damage model for ductile failure in shear. J Mech Phys Solids 58:1243–1252